Available online at www.sciencedirect.com
SCIENCE DIRECT
Polymer 47 (2006) 1281–1290
polymer
www.elsevier.com/locate/polymer

Order and segmental mobility during polymer crystallization: Poly (butylene isophthalate)

Alejandro Sanz [a], Aurora Nogales [a,*], Tiberio A. Ezquerra [a], Nadia Lotti [b], Andrea Munari [b], Sergio S. Funari [c]

[a] *Instituto de Estructura de la Materia, CSIC, C/Serrano 121, Madrid 28006, Spain*
[b] *Dipartamento di Chimica Applicata e Scienze dei Materiali, Universitá di Bologna, Via Risorgimento 2, 40136 Bologna, Italy*
[c] *Max-Planck Intitute for Colloids and Surfaces, c/o HASYLAB, DESY, Notkestraße 85, 22603 Hamburg, Germany*

Received 19 October 2005; received in revised form 3 December 2005; accepted 10 December 2005
Available online 18 January 2006

Abstract

The influence of the development of crystalline structure on the segmental dynamics of the amorphous phase in poly(butylene isophthalate) (PBI) has been studied by a combination of relaxation and scattering techniques. By means of dielectric spectroscopy (DS) the dynamics of both amorphous and semicrystalline PBI samples has been observed in a wide frequency and temperature range. The evolution of the crystalline phase with time has been studied in a range of temperatures, starting from initially glassy PBI by simultaneous small and wide angle X-ray scattering (SWAXS). By using a state-of-the-art setup designed specifically for the in situ study of both DS and SWAXS simultaneously (SWD), the crystallization of initially amorphous PBI has been followed in real time from both the structural and dynamics points of view. The obtained results support a model based on two different regimes on crystallization and a heterogeneous distribution of lamellar stacks. During the first regime the primary stacks cause the apparition of a rigid amorphous phase (RAP), i.e. a phase of amorphous chains lacking segmental motion. During the second regime, however, no more RAP is observed, indicating that the new lamellae that appear during this stage are nearly individual and not forming lamella stacks.

Keywords: Poly(butylene isopththalate); Synchrotron radiation; Dielectric spectroscopy

1. Introduction

Polymer systems may exhibit a rich hierarchical structure when crystallize at temperatures above the glass transition temperature (T_g). Although polymer crystallization has been investigated for many years there are several aspects that still remain controversial [1]. The process of crystallization has been historically studied from the viewpoint of the crystalline structure development [2]. However, polymers never crystallize completely and they always present a complex structure, consisting, at least, of two phases: crystalline and amorphous. Polymer crystals arrange themselves into characteristic units consisting of stacks of laminar crystals intercalated by amorphous less ordered regions. The average distance between the centres of two consecutive crystalline lamella is called long spacing (L_b), and is often used to characterize the lamellar structure. L_b is of the order of various tens of nanometers. In general, small angle X-ray scattering (SAXS) is a very suitable tool to study the development of these arrays of lamella [3]. The, either homogeneous or heterogeneous, nature of the distribution of lamellar stacks in the system has been a subject of extended debate in the last years [1,4–9]. Traditionally, the observation of the crystalline phase evolution has been performed by diffraction techniques [10] and by microscopy techniques [11]. Both methods pay special attention to the crystalline phase, and very little, or non-at all, to the amorphous one. X-ray scattering and transmission electronic microscopy (TEM) experiments in different polymers sometimes have been interpreted invoking the formation of a heterogeneous multiple lamellar population arrangement [4–6]. However, similar studies and recent atomic force microscopy (AFM) and TEM studies seem to favour a view in terms of the formation of a homogeneous lamellar space-filling structure [7–9].

From the point of view of the dynamics of the chains participating in the crystallization process, also controversial

* Corresponding author. Tel.: +34 915616800; fax: +34 915645557.
E-mail address: emnogales@iem.cfmac.csic.es (A. Nogales).

0032-3861/$ - see front matter © 2005 Elsevier Ltd. All rights reserved.
doi:10.1016/j.polymer.2005.12.047

effects have been observed during polymer crystallization. The α-relaxation, that appears at $T > T_g$, is associated to the segmental motions of the chains in the amorphous state. This α-process is highly affected by the presence of lamellar crystals. In this respect, it has been proposed, on the basis of thermal and dielectric analysis, that the formation of a rigid amorphous phase (RAP), i.e. a phase of amorphous chains lacking segmental motion, proposed long time ago [12,13], can be located in the interfacial region between the crystalline lamellae and the inter-lamellar amorphous phase [14,15]. However, dielectric experiments in several polymers [16,17] and direct observation of the crystal–amorphous interface in poly(ethylene terephthalate) by means of AFM seems to indicate that the entire inter-lamellar amorphous phase could be considered as rigid [8].

Dielectric spectroscopy (DS) techniques are widely used to study the dynamics of the amorphous chains in polymeric systems [18]. DS has been used to study, in real time, the modification of the dynamics of the segments in the amorphous phase during crystallization processes [16,19–25].

Recently, a combination of wide and small angle X-ray scattering experiments, performed simultaneously with dielectric measurements has been developed in order to monitor in real time the evolution of both, structure in the crystalline phase and dynamics in the amorphous phase during crystallization processes. Results obtained by this technique, labelled as SWD, show the existence of a rigid amorphous phase (RAP) in PET [17] and in PEN that is located mainly between lamella inside the lamellar stacks [26]. However both, PET and PEN are aromatic polyesters with such a regular molecular structure that crystallization easily takes place above T_g. For this reason, it is generally difficult to distinguish between primary and secondary crystallization events.

In this paper, we have selected poly(butylene isophthalate) (PBI) which is a polyester belonging to the class of the poly(alkylene phthalate)s. The chemical structure of PBI is similar to that of the well-known poly(butylene terephthalate) (PBT), but with the two ester groups located in the 'meta' position of the phenyl group (Fig. 1). As opposed to PBT, PET and PEN, the crystallization of PBI is much slower, allowing to obtain a better control over the crystallization kinetics. Here, we present real time isothermal crystallization experiments during cold crystallization of PBI as revealed by means of simultaneous small-wide angle X-ray scattering and dielectric spectroscopy (SWD) measurements in real time. Provided that this procedure aims to obtain information from both the crystalline and the amorphous phase we attempt to shed additional light about the above unresolved topics.

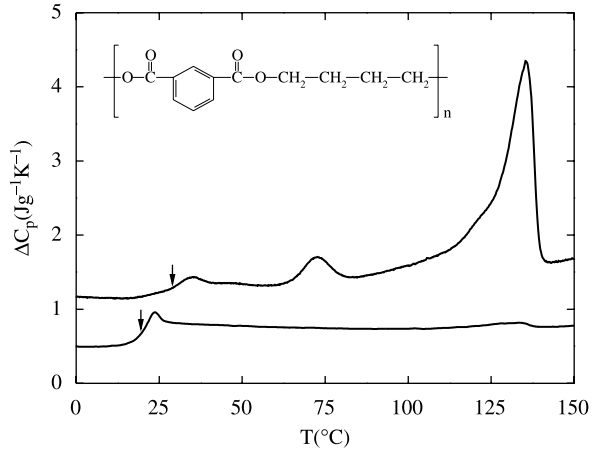

Fig. 1. DSC traces of initially amorphous (bottom) and semicrystalline $X_c = 24\%$ (top) PBI. Arrows indicate T_g.

2. Experimental part

2.1. Samples

Poly(butylene isophthalate) (PBI) was synthesized according to the well-known two-stage polycondensation procedure, as previously reported [27], starting from dimethyl isophthalate and 1,4-butanediol glycol, with titanium tetrabutoxide ($Ti(OBu)_4$) as catalyst. The monomeric unit is presented in Fig. 1. The polymer was previously characterized by some of us from the molecular and thermal point of view [27]. The chemical structure was confirmed by means of ^1H NMR, and the number molecular weight, determined by GPC, turned out to be about 20,000. At room temperature the polymer appeared as a semicrystalline solid. To prepare amorphous films, first the powder obtained from the synthesis was dried under vacuum in order to eliminate existing traces of humidity. Amorphous films of 0.2 mm thickness were obtained by melt pressing the dried powder at $T = 190\,^\circ C$ for 2 min and subsequently quenched into iced water. By this procedure fully amorphous PBI samples are obtained. The specimens were stored at 5 °C before any characterization. The glass transition of this polymer, in the amorphous state is 19 °C, as measured by differential scanning calorimetry (DSC) (Fig. 1). The small tendency to crystallize of PBI is visualize by the absence of exothermal crystallization peak at the current heating rate (10 °C/min). DSC traces obtained in both, the initially amorphous and the semicrystalline sample crystallized at $T =$ 60 °C for 12 h allows one to determine the T_g for each system. Both temperatures are presented in Table 1. The amorphous and semicrystalline samples exhibit a difference in the T_g of approx. 10 °C, being higher in the semicrystalline system.

2.2. Techniques

2.2.1. Differential scanning calorimetry

DSC experiments were carried out with a Perkin–Elmer DSC7 instrument at a heating rate of 10 °C/min. Sub-ambient operation was carried out by using a controlled flow of cooled nitrogen gas by using a Perkin–Elmer TA7. The temperature was calibrated by using indium standard. The samples were encapsulated in aluminium pans and the typical sample weights used in these experiments were about 5 mg.

2.2.2. Dielectric spectroscopy measurements

Dielectric loss measurements (ε'' where $\varepsilon'' = \mathrm{Im}(\varepsilon^*)$) were performed over a broad frequency range (10^{-1}–10^7 Hz) in a

Table 1
Characteristic values for the two studied samples

Sample	T_g^{DSC}(°C)	ΔC_p (J K^{-1} g^{-1})	D	Log(F_0/Hz)	T_0 (K)	$T_{\tau=100\ s}$ (°C)
Amorphous	19.5	0.335	8.3	13.2	236	18
Semicrystalline	29	0.144	7.6	13.2	247	26

T_g and ΔC_p obtained by DSC, and fittings parameters from the VFT equation.

temperature range of $-150\ °C < T < 110\ °C$ using a BDS-40 Novocontrol system with an integrated dielectric interface alpha. The temperature in these experiments was controlled by a nitrogen jet with a temperature error, during every single sweep in frequency, of ± 0.2 °C.

2.2.3. Simultaneous structural and dynamic measurements

Changes in the amorphous and crystalline phases of the system were studied by simultaneous SAXS, WAXS and dielectric spectroscopy experiments. They were performed in the soft condensed matter research beamline A2 at HASYLAB (DESY, Hamburg), using an experimental setup (SWD setup) developed specifically for this purpose [28]. The wavelength used in the X-ray scattering study was $\lambda = 1.5$ Å. The collected data were corrected for background and primary beam intensity fluctuations during the experiment. The dielectric study in the case of the SWD setup was performed using a Novocontrol system integrating a SR830 lock in amplifier with a dielectric interface. A circular film of PBI (3 cm diameter) was sandwiched between two electrodes and introduced in an on-purpose designed cell described elsewhere [28]. Simultaneous wide and small angle X-ray scattering was recorded for 90 s with 90 s wait time between frames. Each dielectric spectrum, obtained simultaneously with the X-ray experiments, took 180 s to collect.

3. Data analysis

3.1. Wide angle X-ray scattering patterns

The crystallinity of the final pattern was obtained as the ratio of the deconvoluted crystalline peaks over the total diffracted area. By this method, the diffraction pattern of the crystalline phase at any moment of the crystallization process was considered fixed in shape, and only its intensity was varied. The contribution of the amorphous halo was taken from the initial pattern (crystallization time $t_c = 0$). Therefore, at any time, the diffraction pattern was considered to be a linear combination of the crystalline contribution (A_c) and the amorphous one (A_a). The crystallinity was obtained by:

$$X_c = \frac{A_c}{A_c + A_a} \tag{1}$$

3.2. Small angle X-ray scattering patterns

The position of the scattering maximum, q_{max}, from the Lorentz-corrected SAXS profile, was used for the calculation of the Bragg's long period, L_B:

$$L_B = \frac{2\pi}{q_{max}} \tag{2}$$

where $q = (4\pi/\lambda)\sin\theta$ is the scattering vector, and 2θ is the scattering angle. L_B corresponds to the average periodicity of the lamellar stack, which corresponds, in first approximation, to the sum of the average thickness of the crystal lamellae, l_c, and of the interlamellar amorphous regions, l_a. However, this method does not readily provide any information about l_a or l_c.The SAXS data have been analyzed using the correlation function approach by Vonk [29] using the methods described by Strobl and Schneider [30]. The electronic density correlation function was calculated from the Fourier transform of the Lorentz-corrected profile using the approximations previously described [16]. The lamellar variables obtained from this analysis of the scattering data are long period (L), linear degree of crystallinity (X_{cL}), crystalline lamellar thickness (l_c) and amorphous layer thickness (l_a). The average linear degree of crystallinity in the lamellar stacks can be determined from the following equation [31]:

$$x_1 x_2 = \frac{B}{L_c^M} \tag{3}$$

where B is the first intercept of the correlation function with the abscissa, L_c^M is the long spacing calculated from the first maximum in the correlation function, and x_1 and x_2 are the volume fractions of the two phases, within the lamellar stacks, respectively ($x_1 + x_2 = 1$). The thickness of the two phases can be calculated as $L_1 = x_1 L_c^M$ and $L_2 = x_2 L_c^M$. From the correlation function itself it is not possible to associate L_1 or L_2 to the thickness of the crystalline lamellae unless a given model is invoked. The principles of the subsequent analysis and the evaluation of the correlation function are discussed in detail elsewhere [31]. Another magnitude that can be derived from the SAXS experiments is the invariant, Q, defined as the area under the SAXS curves.

3.3. Dielectric loss curves

The description of the dielectric relaxation in terms of the Havriliak–Negami empirical equation [32] for the dielectric permittivity has been shown to be of great use when dealing with polymeric materials [18]. This formalism gives the following expression for the complex dielectric permittivity:

$$\varepsilon^* = \varepsilon_\infty + \frac{\varepsilon_0 - \varepsilon_\infty}{[1 + (i\omega\tau_{HN})^b]^c} \tag{4}$$

where ε_0 and ε_∞ are the relaxed and unrelaxed dielectric constant value, respectively, τ_{HN} is the central relaxation time,

and b and c are parameters which describe the symmetrical and asymmetrical broadening of the relaxation time distribution function, respectively. The fact that the α-relaxation is described by an HN equation (Eq. (4)) implies that there is a distribution of relaxation times with most probable value τ_{HN}. The average relaxation time of the relaxation time distribution function is calculated through:

$$\tau = \tau_{HN}\left[\sin\left(\frac{b\pi}{2+2c}\right)\right]^{-1/b}\left[\sin\left(\frac{bc\pi}{2+2c}\right)\right]^{1/b} \quad (5)$$

The difference $\Delta\varepsilon = \varepsilon_0 - \varepsilon_\infty$ is called dielectric strength and it is related to the amount of dipoles involved in the relaxation process.

4. Results

4.1. Dielectric loss spectroscopy of PBI

Fig. 2 shows the dependence of the dielectric loss (ε'') with frequency and temperature. The dielectric spectrum reveals the existence of two main relaxations, as evidenced by the presence of two main maxima that shift towards higher temperatures when the frequency is increased. At low temperatures, a broad maxima located around $F = 10^2$ Hz for $T = -80$ °C indicates the presence of some dynamics with a local character at low temperatures. This maximum is labelled as β-relaxation. At higher temperatures (i.e. at temperatures above the glass transition temperature $T_g = 19$ °C as measured by calorimetric methods) a more intense and narrower maximum is observed, positioned at $F = 10^2$ Hz for $T = 45$ °C. The existence of this maximum is associated to the presence of segmental motions above the T_g. The frequency of maximum loss (F_{max}) has been represented in Fig. 3 as a function of the reciprocal temperature (Arrhenius representation). In this plot, the β-relaxation follows a linear behaviour as corresponds to a local non-cooperative thermally activated process with and activation energy of 44 kJ/mol. The α-relaxation, however, exhibits some curvature, and the dependence of F_{max} with temperature, for this relaxation, can be described by means of the Vogel Fulcher Tamann equation (VFT):

$$F_{max} = F_0 \exp\left[\frac{-DT_0}{(T - T_0)}\right] \quad (6)$$

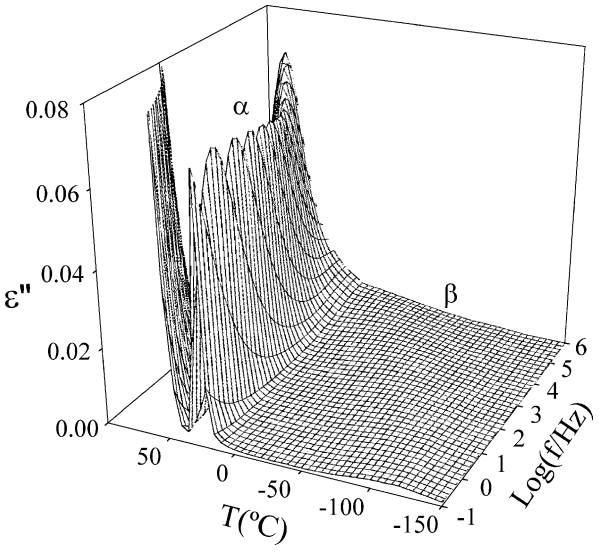

Fig. 2. Dielectric loss (ε'') as a function of frequency and temperature for amorphous PBI.

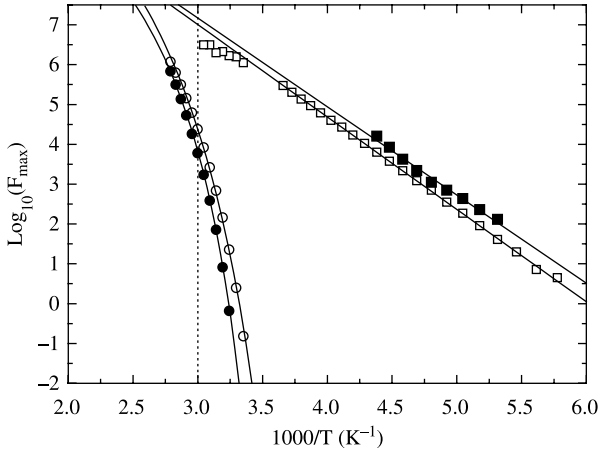

Fig. 3. Relaxation map of PBI: F_{max} as a function of the reciprocal temperature for the two observed relaxations: α (○) and β (□). (●) Correspond to the α-relaxation of the semicrystalline PBI sample. Continuous lines correspond to best fittings according to VFT equation (α-relaxation) and Arrhenius equation (β-relaxation). The dotted line indicates the temperature at which the SWD crystallization experiments were performed.

The α-relaxation of the semicrystalline sample has been also studied by dielectric spectroscopy as a function of temperature and frequency. Fig. 3 shows the variation of the frequency of maximum loss with the reciprocal temperature in an Arrhenius plot, for the amorphous and the semicrystalline sample. As can be observed in that figure, the α-relaxation of both samples exhibit a VFT behaviour. The fit of the experimental points to the VFT equation is also indicated in Fig. 3 with continuous lines, and the obtained parameters are presented in Table 1.

4.2. Isothermal crystallization of PBI as followed by WAXS and SAXS

In order to analyze the influence of crystallization conditions on the structure developed by PBI, simultaneous wide and small scattering experiments were performed isothermally at different temperatures. Fig. 4 shows the evolution of the scattered intensity at wide angle (top) and small angle (bottom) during an isothermal crystallization of PBI at $T = 80$ °C. As a function of time, crystallization is revealed in the WAXS patterns by the onset of several Bragg reflections superimposed to the amorphous halo. In the scattered intensity at small angle (SAXS) the presence of crystals arranged in a periodic fashion is manifested with the development of a maxima located around $q = 0.036$ Å^{-1} for $t_c > 2000$ s. From the WAXS pattern an estimation of the fraction of crystalline phase (X_c) in the sample can be obtained

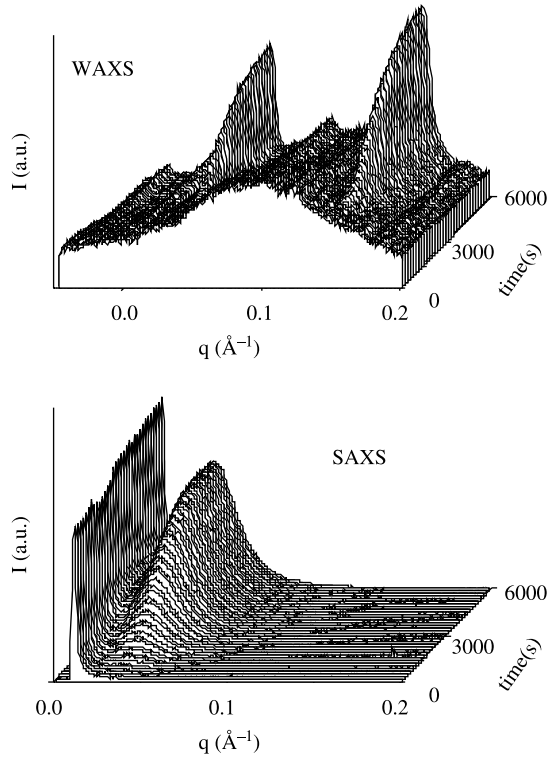

Fig. 4. Isothermal crystallization process at $T=80$ °C as followed by real time simultaneous WAXS (top) and SAXS (bottom).

by deconvoluting the Bragg reflections and the amorphous halo from the total reflections. The evolution with time of X_c, for different temperatures is presented in Fig. 5. There is a strong dependence of the rate of crystallization with temperature. To emphasize this, in the inset of Fig. 5 the half time of crystallization ($t_{1/2}$), defined as the time when the 50% of the maximum crystallinity is reached, is reported as a function of temperature. As it can be seen, the maximum rate of crystallization is observed approx at 90 °C, as previously found by some of us [33].

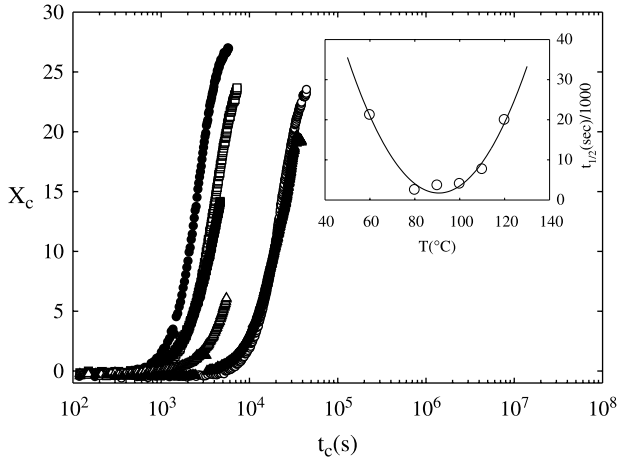

Fig. 5. Evolution of the fraction of crystalline phase (X_c) with time, obtained from the WAXS patterns at different temperatures (○ $T_c=60$ °C, ● $T_c=80$ °C, □ $T_c=90$ °C, ■ $T_c=100$ °C, △ $T_c=110$ °C and ▲ $T_c=120$ °C). The inset represents $t_{1/2}$ as a function of the crystallization temperature T_c.

To characterize any obtained differences in the crystalline nanostructure developed when crystallizing under different temperature conditions, a profound study of the evolution of the SAXS curves has been made by using the formalism of the correlation function, as described previously [16]. The values of the long spacings obtained by direct application of the Bragg law (Eq. (2)) are presented in Fig. 6(a). For a given crystallization temperature, L_b initially decreases with the crystallization time (t_c) up to times $t_c/t_{1/2}\approx 1$ and subsequently it levels off. This behaviour is found for all the studied temperatures, except for the crystallization studied at the highest temperature $T_c=120$ °C. For this temperature L_b remains nearly constant for the whole crystallization process. The obtained final L_b values (for long crystallization times) are higher when the crystallization temperature increases. Moreover, from the analysis of the SAXS curves within the formalism of the correlation function [29,30,34], and assuming that the nanostructural morphology of the system consists of a periodic arrangement of crystalline lamella and amorphous

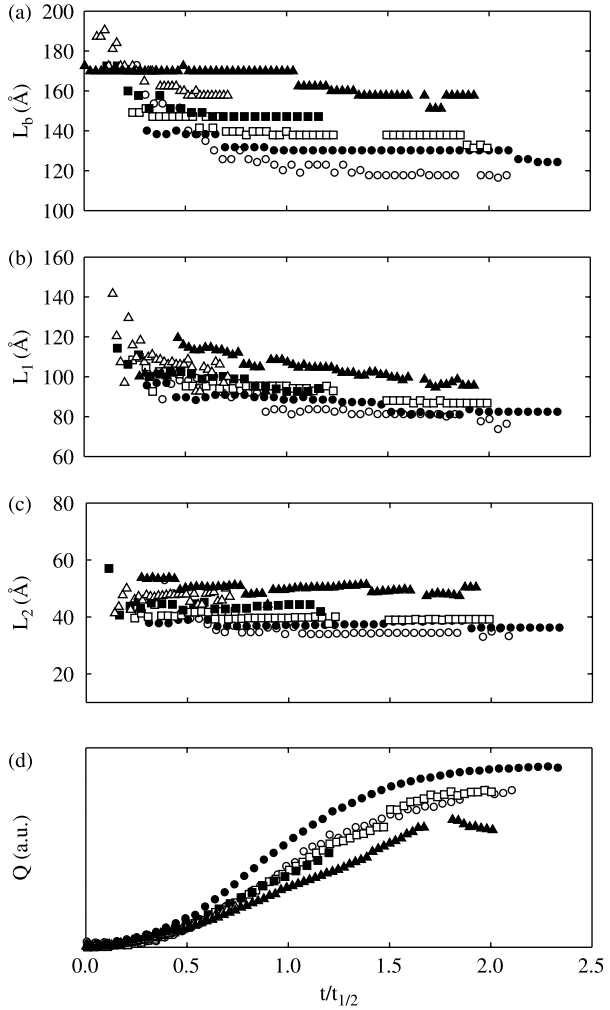

Fig. 6. Evolution of (a) the Bragg long spacing (L_b), (b) and (c) thicknesses of the two constituent phases L_1 and L_2,and (d) invariant Q with time normalized to the half time of crystallization at each temperature (Fig. 5), (○ $T_c=60$ °C, ● $T_c=80$ °C, □ $T_c=90$ °C, ■ $T_c=100$ °C, △ $T_c=110$ °C and ▲ $T_c=120$ °C).

regions, the thicknesses of the two constituent phases (L_1 and L_2) have been obtained. The resulting values are presented in Fig. 6(b) and (c) as a function of the normalized crystallization time ($t_c/t_{1/2}$) for the different studied crystallization temperatures. First of all, it has to be emphasized, that representative values of L_1 and L_2 are obtained only for $t_c/t_{1/2} > 1/2$, where the SAXS curves exhibit a clear maximum and the calculations to obtain the correlation function can be performed with a high degree of confidence. The obtained values for the thickness of one of the phases, L_1, are between 80 and 120 Å in the whole range of crystallization times and temperatures. During every isothermal experiment, L_1 values slightly decrease with t_c. With increasing crystallization temperature, higher L_1 values are obtained. Fig. 6(c) presents the calculated values of L_2, which corresponds to the thickness of the second constituent phase of the lamellar morphology, as function of time and crystallization temperature. The behaviour of L_2 as a function of temperature is similar to that observed for L_1. The higher the temperature at which the isothermal crystallization experiment has been performed, the higher the L_2 obtained values. For L_2 it is worth mentioning that the obtained values in the crystallization at $T_c = 120$ °C are considerably higher than those obtained at the lower crystallization temperatures. With the crystallization time, L_2 tends to be constant, or in some cases, it exhibits a slight increase as crystallization develops.

The calculated invariant is shown in Fig. 6(d). The evolution with time is qualitatively similar to that observed in previous studies for other polymers [16,35].

4.3. Simultaneous WAXS, SAXS and DS experiments

In order to gain information about the changes in the amorphous phase produced by the crystallization process, measurements of the α-relaxation as a function of the crystallization time were performed at a selected crystallization temperature, in this case $T_c = 60$ °C. This temperature was chosen to be located in the left branch side of the $t_{1/2}$ parabolic curve (inset in Fig. 5). Thus, undesirable crystallization previous to the isothermal experiment was prevented. At this temperature the α-relaxation fell within the experimental frequency window ($10^{-1} < F$ (Hz) $< 10^5$) as marked in Fig. 3 by the vertical dotted line, and the characteristic crystallization times allow the study of the structure by means of real time wide and small angle X-ray scattering. Fig. 7 presents the results obtained by using simultaneously the three techniques during the crystallization process. In the left panels of Fig. 7

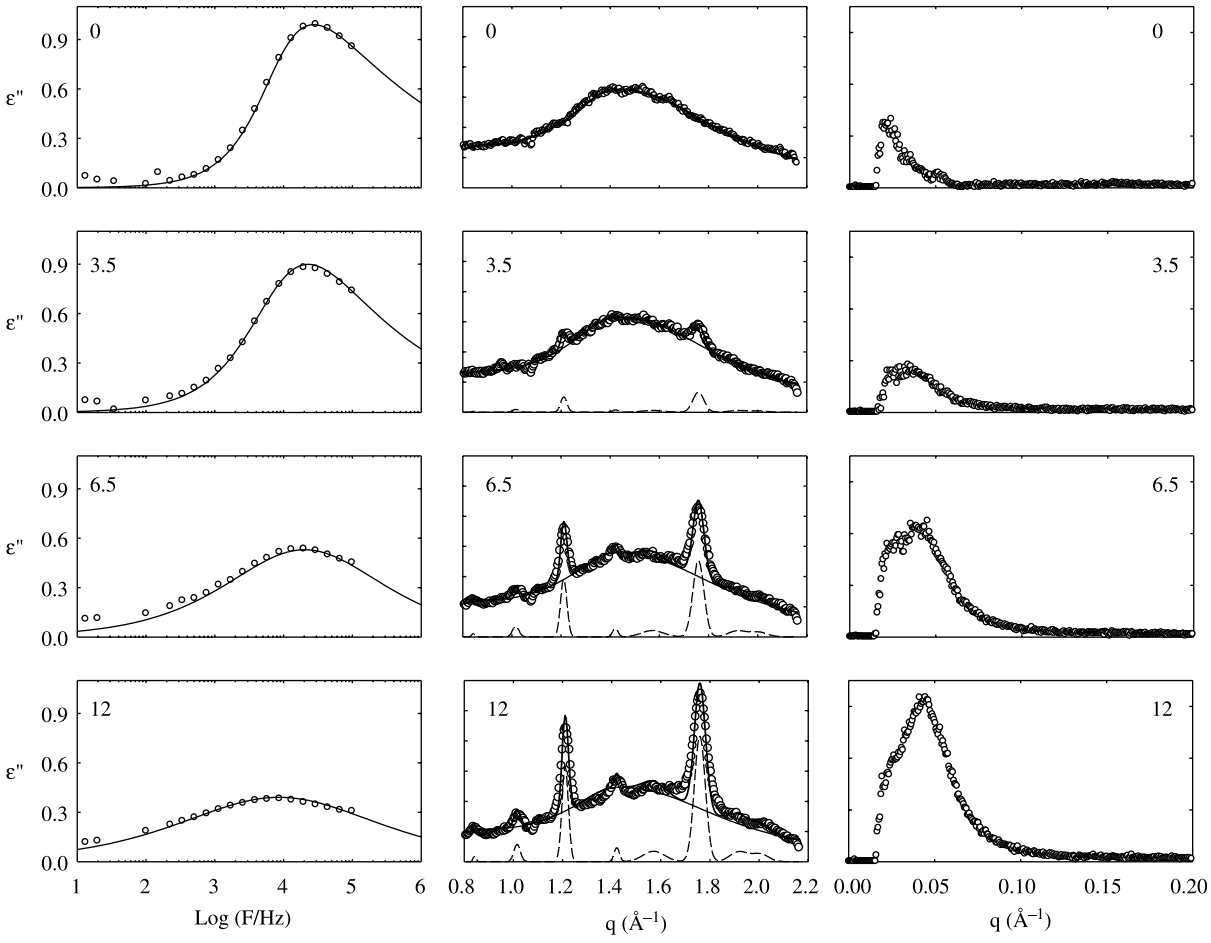

Fig. 7. Evolution of the α-relaxation as measured by DS (left), WAXS (centre) and SAXS (right) during the real time of the crystallization process ($T_c = 60$ °C), at selected crystallization times, labelled within the figures in hours.

values of the dielectric loss (ε'') as a function of frequency for different crystallization times have been represented. SAXS (right panel) and WAXS (centre panel) intensities are presented for the same selected t_c as a function of the scattering vector q. The initial amorphous state is characterized by the presence of a broad halo in the WAXS intensity, the absence of scattering in the SAXS pattern, and by a maximum in ε'' values located at $F_{max}=2\times10^4$ Hz. As time proceeds, the crystallization of PBI starts, as revealed by the incipient growth of Bragg maxima in the WAXS patterns. Especially visible are the ones located at $q=1.20$ and 1.75 Å^{-1}. The crystallization gives rise to the formation of an heterogeneous nanostructure, characterized by the presence of periodicity revealed by the maximum appearing in the SAXS patterns, that in the initial stages is located around $q=0.36$ Å^{-1}. In the DS experiment, the onset of crystallization is revealed by a decrease in the intensity of the relaxation. For longer crystallization times, the features in the WAXS and SAXS patterns that evidenced the presence of crystals arranged in a periodic structure become more pronounced, with more intense Bragg peaks and a more defined SAXS maximum. In this stage of the crystallization process, the α-relaxation process is affected not only in intensity but also in shape and position. The relaxation becomes broader and slightly shifts towards lower frequencies. The dielectric loss curves were analyzed within the Havriliak–Negami phenomenological framework. From this analysis, values of the dielectric strength ($\Delta\varepsilon$), average relaxation time (τ), and shape parameters b and c are obtained. Fig. 8 shows jointly the variation of X_c, L_b and the invariant Q, and the dynamic parameters, $\Delta\varepsilon$, τ and b and c with t_c. $\Delta\varepsilon$ exhibits a nearly sigmoidal decrease with t_c. During the initial stages of the crystallization process $\Delta\varepsilon$ does not vary. Suddenly, it exhibits a dramatic decrease, and for $t_c>t_{1/2}$ it exhibits a change of tendency, with a small slope linear behaviour. The average relaxation time τ presents a different trend with t_c. For $t_c<t_{1/2}$ it remains constant, and for $t_c>t_{1/2}$ increases indicating a slowing down of the relaxation process as crystallization proceeds in its latter stages. Regarding the shape parameters, Fig. 8 shows the variation of the HN parameters defining the shape of the relaxation, with crystallization time. The b parameter, related to the symmetrical broadening of the curve, decreases with crystallization time, indicating that the relaxation time distribution becomes broader. The c parameter increases and it becomes nearly 1 for $t_c\approx t_{1/2}$.

Before discussing the observed results, we present a summary of the observed results.

The study of the isothermal cold crystallization process in PBI at different temperatures reveals that, in all cases, there is a transformation from the totally amorphous state towards a semicrystalline one. A sigmoidal like shape is observed in the evolution of the crystallinity with time at all the studied temperatures. The inset in Fig. 5 shows that as the crystallization temperature varies, dramatic changes in the crystallization rate are produced. At low temperatures, the crystallization is slow while it accelerates by increasing the temperature in the range between 60 and 90 °C. At higher temperatures a slow down is observed. This behaviour was

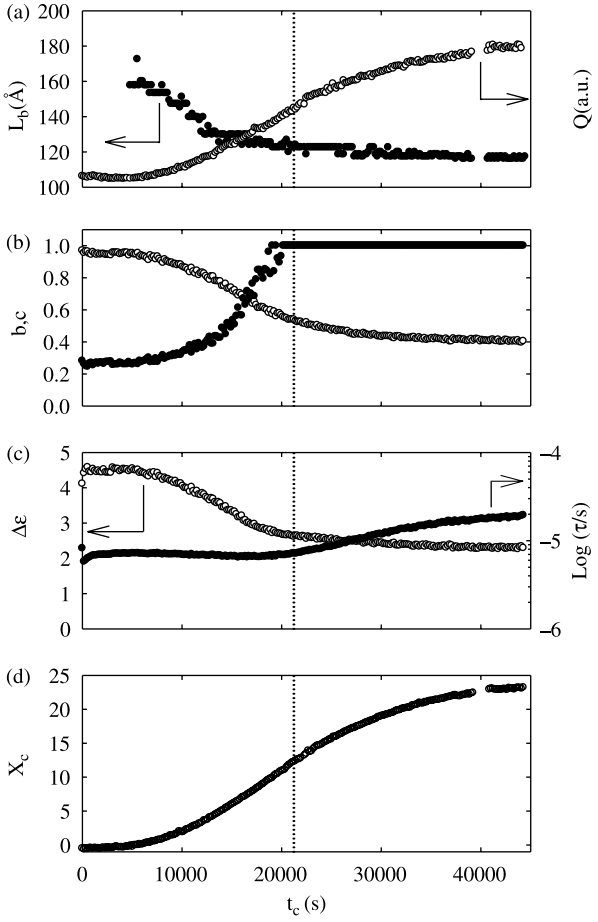

Fig. 8. (a) Variation of the Bragg long spacing (●) and the invariant (○) with the crystallization time. (b) Variation of the shape parameters of the relaxation with crystallization time (○, *b*) and (●, *c*). (c) Variation of the dielectric strength (○) and average relaxation time (●) with time during the crystallization experiment, obtained simultaneously with the SWD technique for PBI crystallizing at $T_c=60$ °C. (d) Variation of the crystallinity with time during the SWD experiment.

previously observed in PBI by means of calorimetric experiments [27]. In all the studied temperatures, after a given induction period, whose length depends on T_c, Bragg peaks start to appear, accompanied by an emerging SAXS maximum. The presence of this maximum suggests the formation of a periodic structure in the range of tenths of nanometers. This periodicity corresponds to crystalline lamellae stacked together and separated by interlamellar amorphous regions. The characteristics of these arrangements of crystals are given by the structural parameters obtained from the analysis of the SAXS curves, and represented in Fig. 6. The dependence of L_b with t_c for each temperature presents similar features at all temperatures. It decreases initially, for $t_c<t_{1/2}$ and then stabilises later on. The final values depend on T_c, indicating that the geometric details of the lamellar stacks formed at different temperatures are different. The repeating distance in the stacks formed at higher temperatures is larger than the one obtained at low temperatures. From the analysis of the correlation function of the SAXS curves it is possible to obtain the fraction of each of the constituent phases x_1 and x_2,

and through that, by using the value of the long spacing, detailed geometrical characteristics of the lamellar stacks, such as the thicknesses of both phases, L_1 and L_2 are obtained (Fig. 6) [36]. Considering those values, one obtain nearly constant values for the fraction of the constituent phases as a function of the crystallization time ($x_1 = 70\%$ and $x_2 = 30\%$, independently of the T_c). The geometrical characteristic of the stacks, however, exhibit a clear dependence with both, crystallization time and temperature. L_1 decreases clearly with t_c, and it presents higher values for the higher T_c. On the contrary, L_2 remains nearly constant during the crystallization process, and also the higher T_c is, the higher the values of L_2 are.

5. Discussion

5.1. Nanostructural development

It has been extensively discussed that, from all the above-mentioned features, it is not possible to assign unambiguosly L_1 and L_2 to either the crystalline lamellae thickness or the interlamellar amorphous regions thicknesses. An additional criterion may arise from the obtained values of crystallinity. In all the studied temperatures, X_c is always around 25%. The correlation function provides values for the fraction of the phases forming the stacks, x_1 and x_2 that are higher than X_c. This implies that, the crystallinity in the stacks is higher than the overall crystallinity, indicating an inhomogeneous distribution of the stacks in the sample. If the higher value of x_1 and x_2 is assigned to the crystalline fraction, then the inhomogeneity of the distribution of the crystals will be higher, indicating that the stacks are highly crystalline and there are broad amorphous areas separating the stacks. On the contrary, if x_2 is considered to be the fraction of crystalline material in the stacks, then the stacks should nearly cover the whole sample, and there will not be broad amorphous areas when the crystallization process is finished. The discussion of the dynamic measurements, presented in the next paragraph, may help to elucidate this question.

5.2. Changes in the segmental dynamics of the amorphous phase induced by the crystalline phase

As mentioned in Section 4, by performing SWD experiments, one obtains parallel information on the structure development and on the changes induced by this development on the dynamics. According to the Kirkwood–Fröhlich equation, at a given temperature, the dielectric strength $\Delta\varepsilon$ in a first approach, assuming a constant dipole correlation, is proportional to the amount of dipoles involved in the relaxation process [37–39]. As evidenced by the SWD experiments, the onset of crystallization produces a strong reduction of the intensity of the relaxation, i.e. of the $\Delta\varepsilon$. Close analysis of this dependence (Fig. 8) shows that in the initial stage of crystallization ($t_c < t_{1/2}$) the reduction in the amount of dipoles involved in the relaxation is drastic. As an example, at $t_c = t_{1/2}$, ($t_{1/2} \approx 20{,}500$ s, dotted lines in Fig. 8), the crystallinity reaches values of around 12.5% whereas $\Delta\varepsilon$ has halved its value. This observation cannot be explained unless one assumes that, the material immobilized during this stage of crystallization comes not only from the chain segments incorporated to the crystals, but also from an extra immobile phase that is not crystalline. This is a clear evidence for the formation of a rigid amorphous phase (RAP) during crystallization. As observed in other polymeric system [16,17], one possibility is that this RAP is located between adjacent lamellae inside the lamellar stacks. During the initial crystallization regime, when the stacks have not impinged with each other, the formation of semicrystalline stacks immobilize the material on them: both the amorphous and the crystalline fractions. Therefore, the α-relaxation observed by dielectric spectroscopy comes from broad amorphous regions between the stacks. Accordingly, our results seem to favour a heterogeneous distribution of lamellar crystals. Previous SWD experiments performed in PET [17,40] have shown the existence of a secondary α-relaxation (α') associated to the segmental motion of a restricted amorphous phase. This α'-relaxation is slower than the original α one, since it appears at lower frequencies, and its strength grows at expenses of the α-relaxation. The secondary α'-process has been attributed to the relaxation of the amorphous chain segments belonging to broad regions in the inter lamellar stack regions [17]. In the case of PET, the relaxation in this regions starts to be restricted due to the appearance of the secondary lamellar stacks which start to be significant for $t_c > t_{1/2}$. For times longer than about $t_{1/2}$ α' coexists with the initial α-process. In the present case for PBI, during the crystallization process no secondary α'-process is detected coexisting with the initial one and the evolution from the segmental dynamics for the fully amorphous sample to that of the semicrystalline specimen can be described by a single α-relaxation process. Qualitatively similar behaviour has been observed in different polymers [16,18,20–23]. This can be understood considering that, after completion of the crystallization process the α-relaxation of the semicrystalline PBI sample is about one order of magnitude slower than the original one (Fig. 8(c)). This difference is about half of that observed in PET for similar values of the final crystallinity [17]. Noteworthy, as for PET, the onset of the dynamic restrictions, as revealed by the shift of τ towards higher values, appears around the inflection point, $t \approx t_{1/2}$, of the X_c curve. As mentioned above, for longer times the appearance of secondary crystals starts to be significant. The influence of secondary crystallization events on the dynamics is further emphasized in Fig. 9. In that plot, the value of $\Delta\varepsilon$, normalized to its initial value, is presented versus crystallinity. $\Delta\varepsilon_{norm}$ can be considered as a measure of the fraction of relaxing species [16]. As observed in Fig. 9, $\Delta\varepsilon_{norm}$ decreases with X_c exhibiting two clear linear tendencies. Initially, $\Delta\varepsilon_{norm}$ presents a slope far away from -1, indicating that, during the initial regime, the immobilized segments are not only the ones included in the crystals, but also a large portion of the non-crystallized segments, further supporting the existence of a rigid amorphous phase. Using Fig. 9, one may have an estimation about the fraction of sample included in the RAP. For $X_c =$

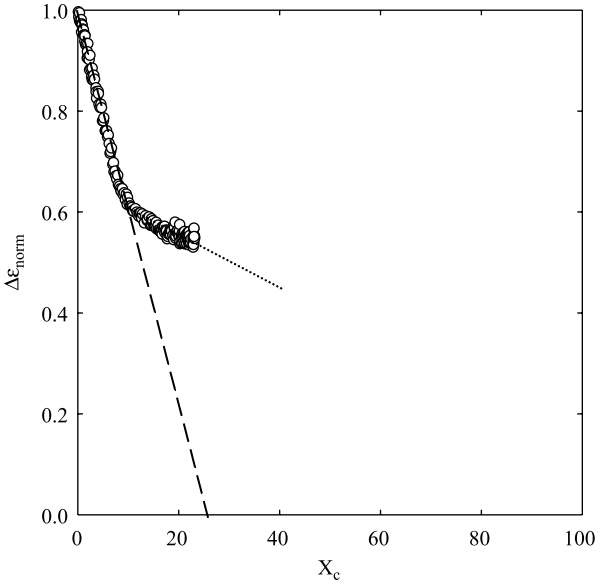

Fig. 9. Normalized dielectric strength $\Delta\varepsilon_{norm}$ as a function of the crystallinity X_c.

10%, $\Delta\varepsilon_{norm}$ indicates that only 61% of the sample experienced the segmental relaxation process. This indicates that there is a 29% of non-crystalline immobile material that can be attributed to the RAP in the system. This value is similar to that obtained by DSC. From the ratio in ΔC_ps of the completely amorphous and semicrystalline samples (Table 1) it is possible to calculate the amount of phase contributing to the glass transition in the semicrystalline sample ($X_{mobile} = \Delta C_p^{sc}/\Delta C_p^{a}$). By this calculation a mobile fraction at T_g of 43% is obtained. Taking into account the 24% of crystallinity estimated by WAXS (in the semicrystalline sample), it leads to a 33% of RAP from the DSC data, in very good agreement with the SWD experiments. Previous results obtained by some of us found the lack of a RAP in crystallized PBI [33]. However, the fraction of interphase depends on the thermal treatment that the material is subjected to, as has been recently observed for poly(propylene terephthalate) (PPT) [41].

For $X_c > 10\%$ the tendency of $\Delta\varepsilon_{norm}$ changes drastically and a second slope ≈ -1 is observed. This can be interpreted assuming that for $X_c > 10\%$ the immobilization of material due to the crystallization process is not as effective as in the previous period. This fact indicates that during secondary crystallization the amount of immobilized material seems to be similar to the amount of material incorporated to the crystals. Thus, one may propose the idea that secondary crystallization in PBI, taking place in the inter stacks amorphous phase does not produce new lamellar stacks but either independent lamellae or very defective stacks. This mechanism should not produce significant amounts of RAP because, as previously discussed, the RAP can be assigned to an intra lamellar stacks amorphous phase. Additional support for this model can be sought in the structural experiments. Formation of new lamellar stacks during secondary crystallization should provoke an overall shift towards lower values of the lamellar

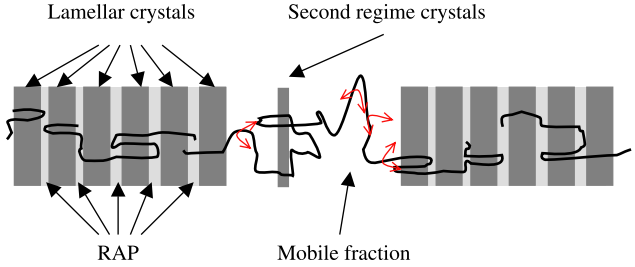

Fig. 10. Schematic drawing illustrating the different fractions present in semicrystalline PBI. The curves arrows represent the segmental motion.

thickness because the secondary lamellar stacks are expected to contain thinner crystals [35]. Additionally, a broadening of the SAXS pattern accompanied by an overall shift towards higher values of L_b should be expected as thinner secondary lamellar stacks appears. In our case, the SWD experiment (Fig. 8(a)) indicates that the long spacing remains essentially constant for $t_c > t_{1/2}$. Moreover, during isothermal crystallization at $T =$ 60 °C neither L_1 nor L_2 exhibit significant changes for $t_c > t_{1/2}$. On the contrary, the formation of new single lamellae in the interlamellar amorphous phase during secondary crystallization should involve no significant changes in the SAXS patterns as it is observed in our case. A similar model has been recently proposed to explain secondary crystallization in poly(ethylene isophthalate-*co*-terephtalate) copolymers crystallized from the melt [42]. Single secondary lamellae should not be capable to anchor the inter lamellar stacks mobile phase as effectively as secondary lamellar stack. This could explain why, for similar crystallinity values segmental dynamics in semicrystalline PET is about two times slower than in amorphous PET [17] where cold secondary crystallization was proposed to proceed by secondary lamellar stacks formation [31,35].

In order to illustrate the proposed model, Fig. 10 presents an schematic drawing of the semicrystalline system at the end of the crystallization process. The lamellar stacks are formed by the alternation of lamellar crystals separated by rigid amorphous areas, where segmental mobility is arrested. Between the stacks, there are broader amorphous regions, where the chains exhibit the α-relaxation. It is in these broader amorphous regions where, during the second regime of crystallization, individual lamellar or defective stacks are formed.

6. Summary and conclusions

Accordingly the combination of the structural and dynamical measurements during the cold crystallization of PBI supports a model based on a heterogeneous distribution of lamellar stacks with relatively broad inter-lamellar stacks amorphous phase where the secondary crystallization takes place. The main derived features from the simultaneous study of the X-ray scattering at wide and small angles and dielectric spectroscopy during the crystallization of PBI are the following:

- There are two clearly differentiated regimes of crystallization: a primary regime where lamellar stacks are formed and a secondary regime in which isolated lamella grow in broad amorphous regions located between the stacks.
- Due to the crystallization in stacks a rigid amorphous phase is formed, which can be assigned to the amorphous fraction included in the stacks, that is, located between consecutive lamella inside the stacks.
- During the second regime of crystallization no more RAP is originated.
- Secondary crystallization proceeds by the formation either of single lamellae or of very defective lamellar stacks.

Acknowledgements

The authors are indebted to MCYT (grant FPA2001-2139) Spain, and Marie Curie Reintegration Grant Program of the European Community (ERG 505674) for generous support of this investigation. The experiments at HASYLAB (Hamburg, Germany) have been supported through the Integrated Infrastructure Initiative 'Integrating Activity on Synchrotron and Free Electron Laser Science' of the European Community-Research Infrastructure Action under the FP6 'Structuring the European Research Area'. A.N. thanks the MCYT for the tenure of a Ramon y Cajal contract. We thank M. Dommach, MJ Capitan and C Alvarez for technical assistance.

References

[1] Sommer JU, Reiter G. Editors lecture notes in physics. Polymer crystallization: observations, concepts and interpretations, vol. 606. Heidelberg: Springer; 2003.
[2] Mandelkern L. Crystallization of polymers. Equilibrium concepts, vol. 1. Cambridge: Cambridge University Press; 2002.
[3] Balta-Calleja FJ, Vonk OC. X-ray scattering of synthetic polymers. Amsterdam: Elsevier; 1989.
[4] Santa Cruz C, Stribeck N, Zachmann HG, Baltá-Calleja FJ. Macromolecules 1991;24(22):5980–90.
[5] Xia Z, Sue H, Wang Z, Avila-Orta CA, Hsiao BS. J Macromol Sci, Phys 2001;B40(5):625–38.
[6] Verma R, Marand H, Hsiao BS. Macromolecules 1996;29(24):7767–75.
[7] Ivanov DA, Legras R, Jonas AM. Macromolecules 1999;32(5):1582–92.
[8] Ivanov DA, Pop T, Yoon DY, Jonas AM. Macromolecules 2002;35(26):9813–8.
[9] Haubruge HG, Jonas AM, Legras R. Macromolecules 2004;37(1):126–34.
[10] Kakudo M, Kasai N. X-ray diffraction by polymers. Amsterdam: Elsevier; 1972.
[11] Bassett DC. Principles of polymer morphology. Cambridge solid state series. Cambridge: Cambridge University Press; 1981.
[12] Cheng SZD, Cao MY, Wunderlich B. Macromolecules 1986;19(7):1868–76.
[13] Hou P, Cebe P. Macromolecules 1992;25(2):902–9.
[14] Dobbertin J, Hensel A, Schick C. J Thermal Anal 1996;47(4):1027–40.
[15] Schick C, Donth E. Phys Scr 1991;43(4):423–9.
[16] Nogales A, Ezquerra TA, Denchev Z, Sics I, Balta Calleja FJ, Hsiao BS. J Chem Phys 2001;115(8):3804–12.
[17] Alvarez C, Sics I, Nogales A, Denchev Z, Funari SS, Ezquerra TA. Polymer 2004;45:3953–9.
[18] Schönhals A, Kremer F. Broad band dielectric spectroscopy. Berlin: Springer; 2002.
[19] Williams G. Adv Polym Sci 1979;33:59–92.
[20] Ezquerra TA, Balta Calleja FJ, Zachmann HG. Polymer 1994;35(12):2600–6.
[21] Nogales A, Ezquerra TA, García JM, Balta Calleja FJ. J Polym Sci, Part B: Polym Phys 1999;37(1):37–49.
[22] Kanchanasopa M, Runt J. Macromolecules 2004;37(3):863–71.
[23] Andjelic S, Fitz BD. J Polym Sci, Part B: Polym Phys 2000;38(18):2436–48.
[24] Mijovic J, Sy JW. Macromolecules 2002;35(16):6370–6.
[25] Massalska-Arodz M, Williams G, Thomas DK, Jones WJ, Dabrowski R. J Phys Chem 1999;3(20):4197–205.
[26] Sics I, Ezquerra TA, Nogales A, Denchev Z, Alvarez C, Funari SS. Polymer 2003;44(4):1045–9.
[27] Munari A, Manaresi P, Chiorboli E, Chiolle A. Eur Polym J 1992;28(1):101–6.
[28] Sics I, Nogales A, Ezquerra TA, Denchev Z, Balta-Calleja FJ, Meyer A, et al. Rev Sci Instrum 2001;71(4):1733–6.
[29] Kortleve G, Vonk CG, Kolloid ZZ. Polymer 1968;225(2):124–31.
[30] Strobl GR, Schneider M. J Polym Sci, Part A-2: Polym Phys 1980;18(6):1343–59.
[31] Hsiao BS, Verma RK. J Synchrotron Radiat 1998;5(1):23–9.
[32] Havriliak S, Negami S. Polymer 1967;8:161–210.
[33] Righetti MC, Pizzoli M, Lotti N, Munari A. Macromol Chem Phys 1998;199(9):2063–70.
[34] Vonk CG, Kortleve G, Kolloid ZZ. Polymer 1967;220(1):19–24.
[35] Wang Z, Hsiao BS, Sauer BB, Kampert WG. Polymer 1999;40(16):4615–27.
[36] Denchev Z, Nogales A, Ezquerra TA, Fernandes-Nascimento J, Balta Calleja FJ. J Polym Sci, Part B: Polym Phys 2000;38(9):1167–82.
[37] Hedvig P. Dielectric spectroscopy of polymers. Bristol: Hilger; 1967.
[38] Fröhlich H. Theory of dielectrics. London: Oxford University Press; 1941.
[39] Fuoss RM, Kirkwood JG. J Am Chem Soc 1941;63:385.
[40] Fukao K, Miyamoto Y. Phys Rev Lett 1997;79(23):4613–6.
[41] Sisti L, Finelli L, Lotti N, Berti C, Munari A. e-Polymers 2003 [Paper no. 54].
[42] Lee B, Shin TJ, Lee SW, Yoon J, Kim J. Macromolecules 2004;37(11):4174–84.